All-Atom Molecular Dynamics Simulation of Protein Translocation through an α-Hemolysin Nanopore

ARTICLE *in* JOURNAL OF PHYSICAL CHEMISTRY LETTERS · JULY 2015

Impact Factor: 7.46 · DOI: 10.1021/acs.jpclett.5b01077

4 AUTHORS, INCLUDING:

Daniele Di Marino
Sapienza University of Rome
23 PUBLICATIONS **346** CITATIONS
SEE PROFILE

Mauro Chinappi
Istituto Italiano di Tecnologia
44 PUBLICATIONS **803** CITATIONS
SEE PROFILE

THE JOURNAL OF PHYSICAL CHEMISTRY Letters

Letter

pubs.acs.org/JPCL

All-Atom Molecular Dynamics Simulation of Protein Translocation through an α-Hemolysin Nanopore

Daniele Di Marino,[†] Emma Letizia Bonome,[‡] Anna Tramontano,[†,§] and Mauro Chinappi*[,∥]

[†]Dipartimento di Fisica, Sapienza Università di Roma, P.le A. Moro, 5, 00185 Rome, Italy

[‡]Dipartimento di Ingegneria Meccanica e Aerospaziale, Sapienza Università di Roma, Via Eudossiana 18, 00184 Rome, Italy

[§]Istituto Pasteur - Fondazione Cenci Bolognetti, Sapienza Università di Roma, Viale Regina Elena 291, 00161 Rome, Italy

[∥]Center for Life Nano Science@Sapienza, Istituto Italiano di Tecnologia, Via Regina Elena 291, 00161, Roma, Italia

Supporting Information

ABSTRACT: Nanopore sensing is attracting the attention of a large and varied scientific community. One of the main issues in nanopore sensing is how to associate the measured current signals to specific features of the molecule under investigation. This is particularly relevant when the translocating molecule is a protein and the pore is sufficiently narrow to necessarily involve unfolding of the translocating protein. Recent experimental results characterized the cotranslocational unfolding of Thioredoxin (Trx) passing through an α-hemolisin pore, providing evidence for the existence of a multistep process. In this study we report the results of all-atom molecular dynamics simulations of the same system. Our data indicate that Trx translocation involves two main barriers. The first one is an unfolding barrier associated with a translocation intermediate where the N-terminal region of Trx is stuck at the pore entrance in a conformation that strongly resembles the native one. After the abrupt unfolding of the N-terminal region, the Trx enters the α-hemolisin vestibule. During this stage, the constriction is occupied not only by the translocating residue but also by a hairpin-like structure forming a tangle in the constriction. The second barrier is associated with the disentangling of this region.

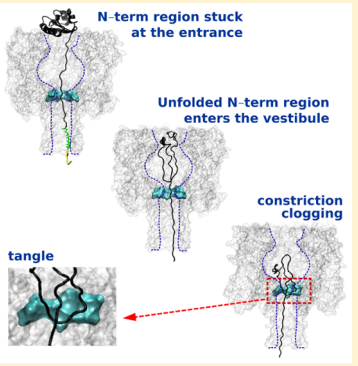

During the past two decades, nanopores have been exploited for the development of new techniques for nucleic acid sequencing,[1−3] and several authors have focused on nucleic acid translocation and on the interpretation of the associated current signal.[4−6] Much less effort has been dedicated to protein and polypeptide sensing.[7−9] Only in the past few years have pioneering single molecule studies appeared in the literature suggesting potentially revolutionary applications in the study of protein (and peptide) sequence and structure.[10−12] Being that the diameters of biological nanopores are too small to allow the passage of polypeptides in their native conformation, protein translocation is necessarily associated with unfolding.[13,14] Early studies have revealed that different types of nanopores, biological or solid state, are able to distinguish between distinct protein (and peptide) folding states, i.e., folded, partially folded, and unfolded.[15−17] Recent experimental data demonstrated that the cotranslocational unfolding process occurs through a multistep mechanism[10,18] characterized by a multilevel current signature. Moreover, the cotranslocational unfolding pathway and the translocation rate were shown to depend upon the direction of the translocation, i.e., whether the protein is pulled into the nanopores from the N- or the C-termini.[18] Furthermore, modifications in the multilevel ionic current signature were associated with the presence of amino acid phosphorylation.[19] Together with the above-mentioned experimental results, various computational studies were also performed and used to describe cotranslocational unfolding,[20−23] even though the experimentally observed translocation process is several orders of magnitude slower than the time scale accessible to atomistic simulations. Specifically, the simulations have provided information on the relationship between the applied force and the translocation speed and on the role of the nanopore diameter and have highlighted the differences between mechanical unfolding and the translocation process.[20−26] To date, the computational studies performed on protein translocation cannot be directly correlated with recent available experimental data since all simulations were performed on simplified model systems.

In this scenario, the work described here creates, for the first time, a bridge between the experimental data that macroscopically explore the nanopore protein translocation mechanism and computational studies that can describe the whole process in atomic detail. We performed all-atom molecular dynamics simulations of the thioredoxin (Trx) translocation across an α-hemolysin pore reproducing the experimental setup used by Rodriguez-Larrea and Bayley.[10,18]

The system consists of two main parts: the Trx-DNA complex and the nanopore. The Trx-DNA complex is constituted by thioredoxin, a linker and a 30-mer oligo(dC)

Received: May 24, 2015
Accepted: July 9, 2015

DOI: 10.1021/acs.jpclett.5b01077
J. Phys. Chem. Lett. 2015, 6, 2963−2968

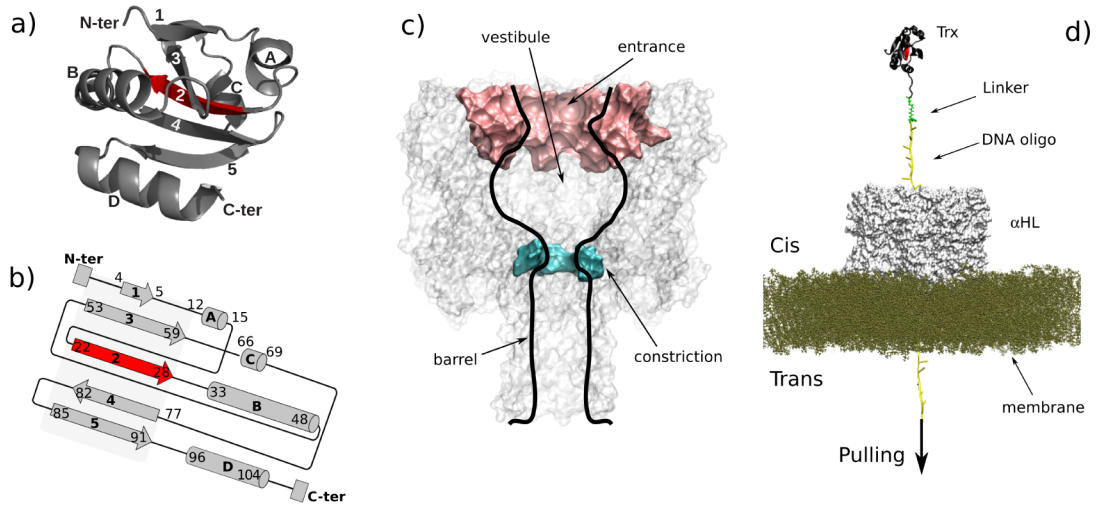

Figure 1. System components and simulation setup. Ribbon representation of Trx 3D structure (a) and its topological diagram[28] (b). The label system used in the text is reported for each secondary structure element (β1 −β5 for β-strands and αA −αD for helices). The α-hemolisin (αHL) structure is sketched in panel c. Constriction residues are shown in cyan, while entrance residues (1−25 of each αHL monomer) are in pink. Panel **d** reports a snapshot of the complete simulated system. Water and ions are not reported for the sake of clarity.

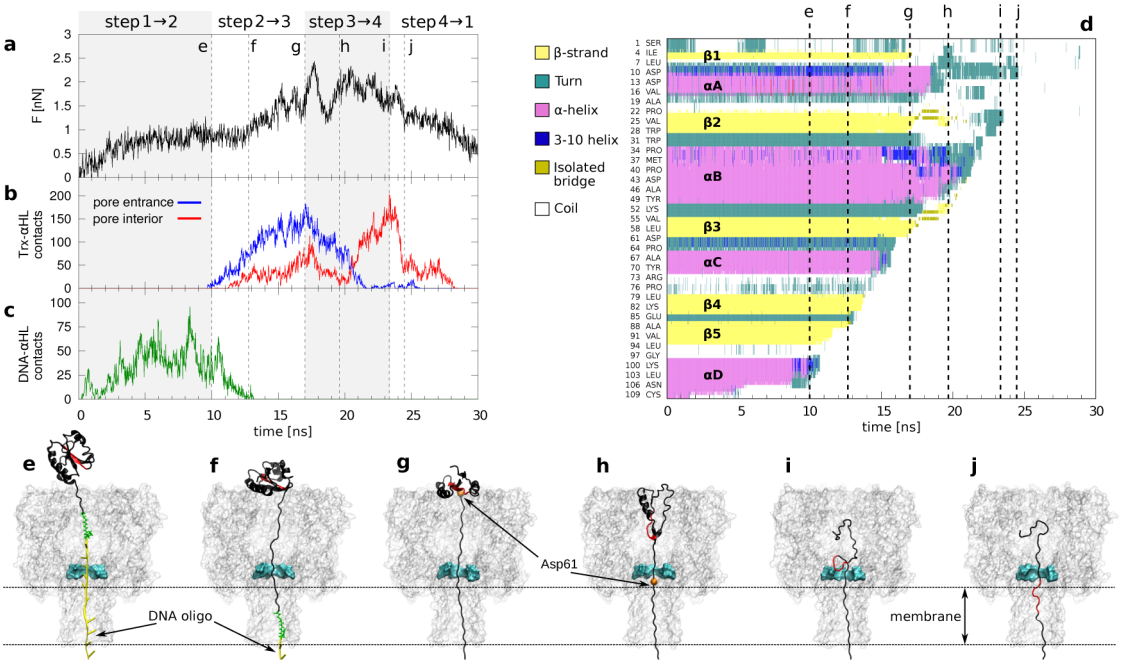

Figure 2. Thioredoxin translocation pathway. (a) Time evolution of the importing force *F*. (b) Number of contacts between Trx and αHL (blue: pore entrance, defined as the residue 1−25 of each chain of αHL, in pink in Figure 1; red: pore interior, i.e., all the αHL but the pore entrance). (c) Number of contacts between DNA and αHL. (d) Time evolution of the secondary structure. Each amino acid is assigned to a secondary structure element using VMD[31,36] while contacts are calculated using the g_mindist tool of Gromacs V. 4.6.3 with a cutoff of 3 Å.[37] (e−j) Snapshots of six representative confomations. Trx residues in the range Ala22-Trp28, corresponding to the β-strand β2 in the native structure, are in red. In step 1 → 2 the DNA is imported into the pore. Trx gradually unfolds and the translocation proceeds as a single-residue transport with the N-terminal portion of Trx stuck at the pore entrance (step 2 → 3). When Asp61 (orange sphere, highlighted only in panels f and g) is at the pore entrance, its translocation is hindered by residues originally belonging to the β2 strand (panel f). This results in a larger force and to a phenomenological change in the translocation process (step 3 → 4). The N-terminal region of Trx completely unfolds, and it is imported in the αHL vestibule (panel g). The number of contacts between the pore interior and Trx increases (panel b) reaching a maximum in conformation i, where an hairpin-like structure occupies the pore constriction. After the passage of this hairpin, the translocation proceeds in a single-residue way and, consequently, both the force (panel a) and the number of contacts with the pore interior (panel b, red curve), decrease.

oligonucleotide leader sequence (in the following, simply indicated as DNA or DNA oligo) connected to the Trx C-terminus, that together form the translocating molecule. In the experiments, the DNA oligo was added to thread the whole complex into the pore. Indeed, when the DNA is inside the pore or close to the pore mouth, it experiences a force due to the electrical field induced by the applied transmembrane voltage. This force also prevents backward movement of the complex. Trx is a globular protein of 108 amino acids composed of four α-helices (Figure 1a,b) and five β-strands

DOI: 10.1021/acs.jpclett.5b01077
J. Phys. Chem. Lett. 2015, 6, 2963−2968

that form a single β-sheet. To make the simulation of the protein translocation as close as possible to the experimental setup, Trx was modified according to the protocol described by Rodriguez-Larrea and Bayley[10,18] (in particular, we use the V5-C109 variant[10]), and the linker molecule is a 5′-thiol-modied cytosine nucleotide that joins the Trx to the DNA oligo. The nanopore is constituted by the α-hemolysin embedded in a dipalmitoylphosphatidylcholine (DPPC) lipid bilayer. This pore is ∼100 Å long, and its interior is constituted by two main regions: the vestibule and the β-barrel (Figure 1c). The vestibule is in the region outside the membrane, and it has a maximum diameter of ∼46 Å. The β-barrel is embedded in the lipid membrane, and it has a cylindrical shape with a diameter of ∼20 Å (computing used the α-carbon). Between these two regions, there is a constriction that constitutes the pore narrowest section[27] (diameter ∼14 Å). The whole resulting system is shown in Figure 1d.

All simulations were performed using the NAMD software[29] and the CHARMM36 force field.[30] System preparation was carried out using using VMD,[31] UCSF Chimera,[32] and the CHARMM-GUI web server.[33] The Protein Data Bank (pdb) structures used were 7AHL[27] and 2TRX[34] for αHL and Trx, respectively. The resulting system is made of 2.1 million atoms. The system was equilibrated in a configuration with the last residue of the Trx-DNA complex (i.e., the last DNA residue) placed at the pore entrance (see Supporting Information for details on the equilibration protocol).

After the equilibration, the atoms of the phosphate group of the lipid molecules were kept harmonically constrained to their equilibrium position. The translocation of Trx was performed by applying a constant velocity pulling[35] on the terminal nucleotide of the DNA leader sequence. In the initial configuration, the whole DNA-Trx complex was on the cis side of the pore, and the terminal residues of DNA leader sequence was aligned with the pore axis. With the employed pulling speed (25 Å/ns), the entire translocation process was accomplished in ∼30 ns. We also performed a constant forcing pulling simulation. The data are reported in the Supporting Information (Figure S1) together with a comment on the different pulling strategies and their connection with the experiments. The cotranslocational unfolding pathway observed in constant force pulling presents the same overall features of those observed using the constant velocity protocol, hence, for the sake of conciseness, we only report the constant velocity pulling data in the paper.

In constant velocity-steered simulation protocol, the main observable employed to identify the different stages of the process is the force F on the pulled residues (Figure 2a). The force F provides information about the barriers encountered during the translocation. Sharp increases in F correspond to large barriers, and the Trx conformations associated with the concomitance of force ramps can be thought as translocation intermediates, i.e., stable conformations that need large pulling force to be translocated across the pore. The identification of the translocation pathway allows a comparison with the experiments by Rodriguez-Larrea and Bayley,[10,18] where the direct observables are the duration and the intensity of the ion current drop. Indeed, the present interpretation of the different current levels observed in the experiments is that translocation is a multistep process where each level is associated with a specific structural arrangement. The duration of each level is, hence, an indirect measure of the barrier experienced by the protein (the larger the duration the larger the barrier). We also monitored the time course of the evolution of the secondary structure elements of Trx (Figure 2d) and of the number of contacts between the construct and different regions of the pore (Figure 2b,c).

The emerging multistep picture is in good agreement with the experimental results by Rodriguez-Larrea and Bayley.[10,18] For this reason, in the description of the different translocation stages, we adopt their notations for the definition of the traslocation steps. In order to introduce the notation, let us briefly recall the Rodriguez-Larrea and Bayley[10,18] findings. They observed four current levels. Level 1 corresponds to the open pore, while levels from 2 to 4 are associated with Trx-DNA complex translocation. The structural rearrangements between the four levels are indicated as steps 1 → 2, 2 → 3, 3 → 4 and, 4 → 1. Level 2 duration is strongly altered by the applied voltage, hence, the authors associated it with the presence of the DNA leader inside the pore (being that the DNA is strongly charged, its translocation is affected by the electrical field inside the pore). Levels 3 and 4 are, instead, due to the presence of Trx inside the pore. The atomistic description of these four processes emerging by our simulation is reported. We performed three replicas; the translocation pathway is the same for all of them. In the main text we refer to only one of them, while data for the other two are reported in the Supporting Information, Figure S2.

Step 1 → 2. The first stage of Trx-DNA translocation is characterized by the single-file transport of the DNA into the pore. As soon as a new DNA residue is imported into the pore, both the number of DNA-αHL contacts (Figure 2c) and the force F (Figure 2a) increase until a plateau is reached at t = 5 ns, i.e., when the pore is completely filled. Pulled by the DNA, Trx approaches the pore maintaining its native folding, with only a limited unfolding of the last part of helix αD (residues Ala105−Ala108; see Figure 2d). Since in this step no unfolding events occur, the force is mainly associated with the friction between the DNA and the pore interior. Step 1 → 2 ends when Trx approaches the entrance (Figure 2e).

Step 2 → 3. Once Trx contacts the pore, the unfolding of helix αD starts ($t \in (10, 12)$ns, Figure 2d). During this period, no changes in the force are observed (Figure 2a). The number of contacts between Trx and the entrance region slightly increases when the DNA exits from the pore. At about t = 12 ns, the force starts to increase (Figure 2a). In this stage, the protein is stuck at the pore mouth (Figure 2f and g) as testified by the large number of contacts between Trx and the pore entrance (Figure 2b, blue line) and progressively unfolds (see the β5, β4 and, αC evolutions in Figure 2d). The unfolding and the traslocation of β5 and β4 break the hydrogen bond pattern that sustains the β-sheet. This is the main reason for the observed increase in the importing force F: the force not only has to compensate the friction between the translocationg residues and the pore interior, but also has to break the native contacts in the C-terminal region of Trx.

Figure 2g shows the conformation before the last ramp in the force curve corresponding to the maximum number of contacts between Trx and the pore entrance. In this figure, Asp61 is highlighted as an orange sphere, and it is at the pore mouth. The sharp force increase after the conformation shown in Figure 2g is associated with the beginning of the unfolding of strand β3 (Figure 2d). Indeed, due to its pivotal position, the unfolding of β3 and its progressive migration into the pore vestibule cause the loss of the hydrogen bonding pattern with both β1 and β2 that become unstructured as well ($t \sim$ 18 ns).

DOI: 10.1021/acs.jpclett.5b01077
J. Phys. Chem. Lett. 2015, 6, 2963−2968

Remarkably, Rodriguez-Larrea and Bayley[18] have proposed that the unfolding intermediate associated with the current level 3 corresponds to the N-terminal portion of Trx stuck at the pore entrance. They hypothesize that step 2 → 3 is a single unfolding event that involves a segment of ∼40 amino acids that goes from the C-terminal to residue Ile60. Our simulations definitely confirm this scenario, indicating that the conformation reported in Figure 2g is representative of the actual translocation intermediate.

Step 3 → 4. The migration of β3 into the pore vestibule triggers the unfolding of β2. As soon as β2 unfolds, the whole portion of the protein at the pore entrance looses the native Trx tertiary structure. This allows the protein to be completely threaded into the pore vestibule (Figure 2h). The penetration of the whole N-terminal portion of Trx into the vestibule is also apparent from the number of contacts between Trx and the pore (Figure 2b).

After a sharp drop ($t \simeq 18.5$ ns), F increases again. However, now the large force is not due to an unfolding barrier but to the interaction with the pore walls of the vestibule and the constriction. Indeed, here we observe no residual secondary structure elements (Figure 2i). This facilitates the interaction of Trx with the internal surface of the pore. As a matter of fact, the number of Trx contacts with the pore interior increases, while a significant drop is observed in the Trx-pore entrance contacts (Figure 2b). The protein is dragged toward the pore constriction. Here a qualitative change in the translocation occurs. Residues Ala22−Trp28, originally belonging to β2 (reported in red in Figure 2e−j), assume an hairpin-like structure, forming a small tangle close to the constriction (Figure 2h). Hence the constriction is not only occupied by the translocating residues, as in the other stages of the translocation, but also by residues in the region Ala22−Trp28.

Our simulation does not allow one to select a specific conformation to be clearly identified as the translocation intermediate for level 4. Indeed, as suggested by ref 18, the protein is largely unfolded, and several small structural rearrangements occur. The only common ingredients of the observed structure are the complete unfolding of the N-terminal region, the interaction with the pore walls, and the tangling of untranslocated residues in the constriction. In the replica reported in the main text and in one of the other two replicas, these residues are in the range Ala22−Trp28 (originally belonging to β2), while in the third replica the clogging residues belong to the turn between αA and β2 (Val16−Ala22).

Step 4 → 1. Once Ala22−Trp28 complete their translocation (sharp drop in the Trx-pore contacts, Figure 2b), the constriction is again only occupied by a single residue (Figure 2j). This single file transport is associated with a decrease in the force that approaches the single-file values, $F \simeq 1$ nN, observed in the early stage of the translocation (step 1 → 2).

Rodriguez-Larrea and Bayley[18] reported that the duration of level 4 is not influenced by the presence of denaturant and, consequently, deduced that, differently from the level 3 intermediate, the conformations associated with level 4 do not involve folded structures. Our simulations confirm this scenario. Moreover, our data indicate that the barrier associated with step 4 → 1 is presumably due to the clogging of the constriction by the hairpin formed by residues in the range Ala22−Trp28. A video showing the above-described cotranslocational unfolding pathway can be found in the Supporting Information.

Summarizing, the data indicate that the Trx translocation process involves two main barriers. The first one (step 3 → 4) is an unfolding barrier associated with a translocation intermediate where the N-terminal region of Trx is stuck at the pore entrance in a conformation that strongly resembles the native one, and the pore constriction is only occupied by a single residue (Figure 2f). The passage of Asp61 drags β3 into the pore (higher peak in force curve) causes the complete unfolding of the N-terminal region of Trx. At this point, the unfolded N-terminal portion of Trx easily migrates into the pore vestibule (Figure 3c) until Trx gets stuck at the

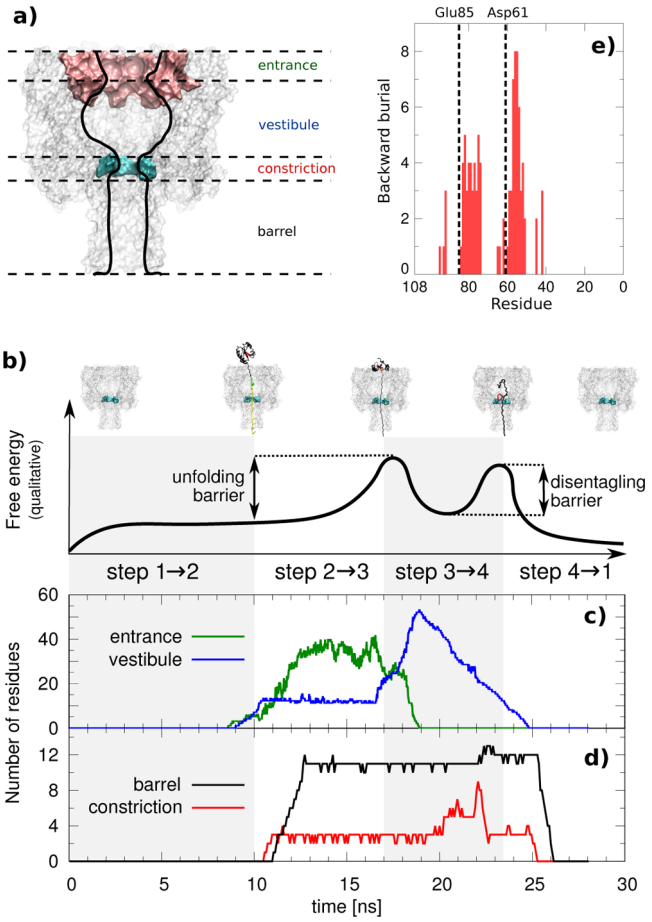

Figure 3. Translocation barriers. The qualitative free-energy profile is sketched in panel b. Panels c and d report the time evolution of the number of residues in the four αHL regions highlighted in panel a. In panel e, the backward burial is plotted as a function of the residue number. The two main peaks are associated with Glu85 and Asp61 that trigger the translocation of α4 and β3, respectively.

constriction. Residues in the region Ala22−Trp28, originally belonging to β2, partially hinder the translocation by clogging the pore constriction. Remarkably, during this stage, the constriction is occupied not only by the translocating residue but also by an hairpin-like structure formed by the Ala22−Trp28 residues (see Figure 2h and Figure 3d). The second barrier (step 4 → 1) is associated with the disentangling of this region. A sketch of the qualitative free-energy profile associated with the observed translocation pathway is plotted in Figure 3b, while Figure 3c,d reports the time course of the number of Trx residues in four regions (entrance, vestibule, constriction, and

DOI: 10.1021/acs.jpclett.5b01077
J. Phys. Chem. Lett. 2015, 6, 2963−2968

barrel) of αHL. It is apparent that in the last part of step 3 → 4 the constriction is occupied by a larger number of residues.

Since the first barrier is associated with the unfolding of native structure elements, it is worth verifying whether this first translocation intermediate can be predicted on the sole base of native structure analysis. It was recently shown that a simple but powerful quantity to predict the translocation intermediates is the backward burial.[13] The backward burial of a given residue is the number of long-range native contacts with the untranslocated chain portions and, in essence, is a measure of the interaction of a residue with the untranslocated portion of the proteins, assumed in a folded state. Figure 3e reports the backward burial as a function of the residue index. Two main peaks are apparent: one associated with the region upstream Glu85 and the other, the largest one, corresponding to Asp61. The latter is clearly associated with the above-discussed unfolding barrier. Indeed the high backward burial is due to the large number of native contacts between β3 and the rest of the N-terminal region. The first peak (Glu85) corresponds to the first increase observed in the force start of the step 2 → 3, and, from a structural point of view, is due to the translocation of α4, $t \simeq 13$ ns.

The translocation mechanism and consequently the multistep unfolding process we observe for the Trx-DNA complex we simulated, can be linked to the data reported by Rodriguez-Larrea and Bayley regarding the mutants K96A and K90D/K96D.[10] In the experiment, K96A and K90D/K96D mutants cause a large increase in step 2 → 3 rate. Our data indicate that step 2 → 3 corresponds to the progressive unfolding of the C-terminus, while the N-terminus region is in the native state and, hence, support the interpretation that destabilizing mutation on the C-terminal region (such as K96A and K90D/K96D) has a large effect on the step 2 → 3 rate, while relatively small effects are observed for step 3 → 4 and step 4 → 1.

We also compared the Trx-DNA translocation pathway with its mechanical unfolding without the pore. The simulation was performed using a standard AFM-like protocol, i.e., fixing the N-terminal residue and pulling the C-terminal residue of the Trx-DNA complex (see Supporting Information). In the AFM-like unfolding simulations (see Figure S3), the first regions to unfold are the two terminals (Ser1−Leu7 and Asp104−Ala108). Then the C-terminal portion, up to Asp61, gradually unfolds. At this point the C-terminal unfolding stops and the next secondary structure element to be lost is αA (Asp10-Ala19). The last part of the process involves the unfolding of β2, β3, and αB. In essence, with the exception of the small initial unfolding of the N-terminal, the mechanical unfolding is characterized by two main stable structural subunits (termed *unfoldons*[38]), the boundary of which is the loop in the region Leu58-Asp61. It is apparent that the translocation and unfolding pathways share some specific features, such as the block at Asp61 and the fact that the last secondary structure element to be lost is αB. However, since partially folded structure cannot enter inside the channel vestibule, the pore imposes an order in the unfoding mechanism (the first structures to unfold are the first to translocate) that is not observed in the AFM-like pulling where, at low forcing, the first structures to break are the weakest ones, independently of their position in the chain.[39] An analogous scenario emerged also from coarse-grained simulations studies, comparing AFM-like and cotraslocational unfolding for other proteins.[21,23]

In conclusion, in this work we show, for the first time, all-atom MD simulations closely reproducing an experimental setup for cotranslocational unfolding.[10] Our data describe the whole process in atomic detail, suggesting a reasonable interpretation of the experimental data. In particular, we are in the position to propose a specific interpretation of the multistep dynamics observed in the experimental setup.[10]

■ ASSOCIATED CONTENT

Supporting Information

A video showing the Trx translocation, details on computational methods, AFM-like unfolding, selected data for the two constant velocity simulation replicas, and results for constant force simulation are reported in the Supporting Information. The Supporting Information is available free of charge on the ACS Publications website at DOI: 10.1021/acs.jpclett.5b01077.

■ AUTHOR INFORMATION

Corresponding Author

*E-mail: mauro.chinappi@iit.it.

Notes

The authors declare no competing financial interest.

■ ACKNOWLEDGMENTS

This research used the computational resource of the Supercomputing Laboratory at King Abdullah University of Science & Technology (KAUST) in Thuwal, Saudi Arabia, and of the CINECA (GRAPUNA project) and PRACE project 2014112673. Funding: KAUST Award No. KUK-I1-012-43 made by King Abdullah University of Science and Technology (KAUST).

■ REFERENCES

(1) Jain, M.; Fiddes, I. T.; Miga, K. H.; Olsen, H. E.; Paten, B.; Akeson, M. Improved Data Analysis for The MinION Nanopore Sequencer. *Nat. Methods* **2015**, *12*, 351.

(2) Schneider, G.; Dekker, C. DNA Sequencing with Nanopores. *Nat. Biotechnol.* **2012**, *30*, 326−328.

(3) Mikheyev, A. S.; Tin, M. M. A First Look at the Oxford Nanopore MinION Sequencer. *Mol. Ecol. Resour.* **2014**, *14*, 1097−1102.

(4) Guy, A. T.; Piggot, T. J.; Khalid, S. Single-stranded DNA within Nanopores: Conformational Dynamics and Implications for Sequencing; a Molecular Dynamics Simulation Study. *Biophys. J.* **2012**, *103*, 1028−1036.

(5) Chinappi, M.; Casciola, C. M.; Cecconi, F.; Marconi, U. M. B.; Melchionna, S. Modulation of Current through a Nanopore Induced by a Charged Globule: Implications for DNA-docking. *EPL (Europhysics Letters)* **2014**, *108*, 46002.

(6) Fyta, M. G.; Melchionna, S.; Kaxiras, E.; Succi, S. Multiscale Coupling of Molecular Dynamics and Hydrodynamics: Application to DNA Translocation through a Nanopore. *Multiscale Model. Simul.* **2006**, *5*, 1156−1173.

(7) Bayley, H.; Cremer, P. S. Stochastic Sensors Inspired by Biology. *Nature* **2001**, *413*, 226−230.

(8) Howorka, S.; Siwy, Z. Nanopore Analytics: Sensing of Single Molecules. *Chem. Soc. Rev.* **2009**, *38*, 2360−2384.

(9) Majd, S.; Yusko, E. C.; Billeh, Y. N.; Macrae, M. X.; Yang, J.; Mayer, M. Applications of Biological Pores in Nanomedicine, Sensing, and Nanoelectronics. *Curr. Opin. Biotechnol.* **2010**, *21*, 439−476.

(10) Rodriguez-Larrea, D.; Bayley, H. Multistep Protein Unfolding during Nanopore Translocation. *Nat. Nanotechnol.* **2013**, *8*, 288−295.

(11) Oukhaled, A.; Bacri, L.; Pastoriza-Gallego, M.; Betton, J.-M.; Pelta, J. Sensing Proteins through Nanopores: Fundamental to Applications. *ACS Chem. Biol.* **2012**, *7*, 1935−1949.

DOI: 10.1021/acs.jpclett.5b01077
J. Phys. Chem. Lett. 2015, 6, 2963−2968

(12) Nivala, J.; Marks, D. B.; Akeson, M. Unfoldase-mediated Protein Translocation through an α-hemolysin Nanopore. *Nat. Biotechnol.* **2013**, *31*, 247−250.
(13) Bacci, M.; Chinappi, M.; Casciola, C. M.; Cecconi, F. Protein Translocation in Narrow Pores: Inferring Bottlenecks from Native Structure Topology. *Phys. Rev. E* **2013**, *88*, 022712.
(14) Pastoriza-Gallego, M.; Breton, M.-F.; Discala, F.; Auvray, L.; Betton, J.-M.; Pelta, J. Evidence of Unfolded Protein Translocation through a Protein Nanopore. *ACS Nano* **2014**, *8*, 11350−11360.
(15) Merstorf, C.; Cressiot, B.; Pastoriza-Gallego, M.; Oukhaled, A.; Betton, J.-M.; Auvray, L.; Pelta, J. Wild type, Mutant Protein Unfolding and Phase Transition Detected by Single-nanopore Recording. *ACS Chem. Biol.* **2012**, *7*, 652−658.
(16) Madampage, C.; Tavassoly, O.; Christensen, C.; Kumari, M.; Lee, J. Nanopore Analysis: An Emerging Technique for Studying the Folding and Misfolding of Proteins. *Prion* **2012**, *6*, 110−118.
(17) Mereuta, L.; Roy, M.; Asandei, A.; Lee, J. K.; Park, Y.; Andricioaei, I.; Luchian, T. Slowing down Single-molecule Trafficking through a Protein Nanopore Reveals Intermediates for Peptide Translocation. *Sci. Rep.* **2014**, *4*, 3885.
(18) Rodriguez-Larrea, D.; Bayley, H. Protein Co-translocational Unfolding Depends on the Direction of Pulling. *Nat. Commun.* **2014**, *5*, 4841.
(19) Rosen, C. B.; Rodriguez-Larrea, D.; Bayley, H. Single-molecule Site-specific Detection of Protein Phosphorylation with a Nanopore. *Nat. Biotechnol.* **2014**, *32*, 179.
(20) Tian, P.; Andricioaei, I. Repetitive Pulling Catalyzes Co-translocational Unfolding of Barnase during Import through a Mitochondrial Pore. *J. Mol. Biol.* **2005**, *350*, 1017−1034.
(21) Huang, L.; Kirmizialtin, S.; Makarov, D. Computer Simulations of the Translocation and Unfolding of a Protein Pulled Mechanically through a Pore. *J. Chem. Phys.* **2005**, *123*, 124903.
(22) Wells, D. B.; Abramkina, V.; Aksimentiev, A. Exploring Transmembrane Transport through alpha-hemolysin with Grid-steered Molecular Dynamics. *J. Chem. Phys.* **2007**, *127*, 125101.
(23) Bacci, M.; Chinappi, M.; Casciola, C.; Cecconi, F. Role of Denaturation in Maltose Binding Protein Translocation Dynamics. *J. Phys. Chem. B* **2012**, *116*, 4255−4262.
(24) Cecconi, F.; Bacci, M.; Chinappi, M. Protein Transport Across Nanopores: A Statistical Mechanical Perspective From Coarse-Grained Modeling and Approaches. *Protein and peptide letters* **2014**, *21*, 227−234.
(25) Bonome, E. L.; Lepore, R.; Raimondo, D.; Cecconi, F.; Tramontano, A.; Chinappi, M. Multistep Current Signal in Protein Translocation through Graphene Nanopores. *J. Phys. Chem. B* **2015**, *119*, 5815.
(26) Wojciechowski, M.; Szymczak, P.; Carrión-Vázquez, M.; Cieplak, M. Protein Unfolding by Biological Unfoldases: Insights from Modeling. *Biophys. J.* **2014**, *107*, 1661−1668.
(27) Song, L.; Hobaugh, M. R.; Shustak, C.; Cheley, S.; Bayley, H.; Gouaux, J. E.; et al. Song, Langzhou and Hobaugh, Michael R and Shustak, Christopher and Cheley, Stephen and Bayley, Hagan and Gouaux, J Eric and others Structure of Staphylococcal Alpha-hemolysin, a Heptameric Transmembrane Pore. *Science* **1996**, *274*, 1859−1865.
(28) Stivala, A.; Wybrow, M.; Wirth, A.; Whisstock, J. C.; Stuckey, P. J. Automatic Generation of Protein Structure Cartoons with Pro-origami. *Bioinformatics* **2011**, *27*, 3315−3316.
(29) Phillips, J. C.; Braun, R.; Wang, W.; Gumbart, J.; Tajkhorshid, E.; Villa, E.; Chipot, C.; Skeel, R. D.; Kale, L.; Schulten, K. Scalable Molecular Dynamics with NAMD. *J. Comput. Chem.* **2005**, *26*, 1781−1802.
(30) Vanommeslaeghe, K.; Hatcher, E.; Acharya, C.; Kundu, S.; Zhong, S.; Shim, J.; Darian, E.; Guvench, O.; Lopes, P.; Vorobyov, I.; et al. Vanommeslaeghe, Kenno and Hatcher, Elizabeth and Acharya, Chayan and Kundu, Sibsankar and CHARMM General Force Field: A Force Field for Drug-like Molecules Compatible with the CHARMM All-atom Additive Biological Force Fields. *J. Comput. Chem.* **2010**, *31*, 671−690.
(31) Humphrey, W.; Dalke, A.; Schulten, K.; et al. Humphrey, William and Dalke, Andrew and Schulten, Klaus and others VMD: Visual Molecular Dynamics. *J. Mol. Graphics* **1996**, *14*, 33−38.
(32) Pettersen, E. F.; Goddard, T. D.; Huang, C. C.; Couch, G. S.; Greenblatt, D. M.; Meng, E. C.; Ferrin, T. E. UCSF Chimera − a Visualization System for Exploratory Research and Analysis. *J. Comput. Chem.* **2004**, *25*, 1605−1612.
(33) Jo, S.; Kim, T.; Iyer, V. G.; Im, W. CHARMM-GUI: a Web-based Graphical user Interface for CHARMM. *J. Comput. Chem.* **2008**, *29*, 1859−1865.
(34) Katti, S. K.; LeMaster, D. M.; Eklund, H. Crystal Structure of Thioredoxin from Escherichia coli at 1.68 Å Resolution. *J. Mol. Biol.* **1990**, *212*, 167−184.
(35) Isralewitz, B.; Gao, M.; Schulten, K. Steered Molecular Dynamics and Mechanical Functions of Proteins. *Curr. Opin. Struct. Biol.* **2001**, *11*, 224−230.
(36) Frishman, D.; Argos, P. Knowledge-based Protein Secondary Structure Assignment. *Proteins: Struct., Funct., Genet.* **1995**, *23*, 566−579.
(37) Hess, B.; Kutzner, C.; Van Der Spoel, D.; Lindahl, E. GROMACS 4: Algorithms for Highly Efficient, Load-balanced, and Scalable Molecular Simulation. *J. Chem. Theory Comput.* **2008**, *4*, 435−447.
(38) Guardiani, C.; Marino, D. D.; Tramontano, A.; Chinappi, M.; Cecconi, F. Exploring the Unfolding Pathway of Maltose Binding Proteins: An Integrated Computational Approach. *J. Chem. Theory Comput.* **2014**, *10*, 3589−3597.
(39) Plata, C. A.; Cecconi, F.; Chinappi, M.; Prados, A. Understanding the Dependence on the Pulling Speed of the unfolding pathway of proteins. *arXiv.org, e-Print Arch., Condens. Matter* **2015**, No. arXiv:1507.01376.

DOI: 10.1021/acs.jpclett.5b01077
J. Phys. Chem. Lett. 2015, 6, 2963−2968